Clean Energy Conversion Research Section
(Two-dimensional tunnel FET)

Kosuke Nagashio, Visiting Professor
(The University of Tokyo)

1. Introduction

For the 2D/2D interfacial properties in TFET, the defect-free clean heterointerface is critical for obtaining the BTBT dominant current under reverse bias at the diode. Although the BTBT current has been demonstrated at low temperatures [1], thermally activated behavior often appears at higher temperatures near RT. That is, the generation current governs the total current, resulting in degradation of the SS at RT. This suggests that interface states exist even for 2D/2D interfaces. In general, high-*k* top gate oxides have been used in most of 2D TFETs reported thus far to enhance the gate capacitance. However, how the quality of the 2D/2D interface is affected by the deposition of high-*k* oxides has not been revealed yet. Therefore, comparisons between high-*k* and *h*-BN gate insulators should be carried out systematically in the same 2D TFET system because the use of *h*-BN in TFETs has been quite limited.

In this work, we systematically studied all 2D heterostructure TFETs produced by combining the type III *n*-MoS_2/p^+-MoS_2 heterostructure with the *h*-BN top gate in order to achieve SS values less than 60 $mVdec^{-1}$ at RT.

2. Strategy in 2D/2D TFET structure

There are three strategies to further reduce the SS values: (i) Recently, we have discovered that the deposition of Al_2O_3 top gate oxide on the MoS_2 channel increases the interface states density due to the introduction of strain in the MoS_2 channel on the *h*-BN substrate, as shown in Fig. 1.[2] Therefore, an *h*-BN top gate insulator was adopted to benefit from the electrically inert interface in 2D heterostructure TFETs. (ii) The p^+-MoS_2 source was used because the E_F of p^+-MoS_2 cannot be modulated due to the degenerately high doping of the p^+-MoS_2. (iii) According to the transmission probability calculated for carrier transport through the BTBT barrier,[3] the E_G for the channel should be larger than that for the source to keep the off current low but E_G also should be as small as possible to increase the transmission probability. Therefore, the 1L and 3L MoS_2 channels were compared. Based on these three considerations, all 2D heterostructure TFETs were fabricated to achieve SS values lower than 60 $mVdec^{-1}$.

3. Results & Discussion

Fig. 2 shows a schematic (a) and an optical micrograph (b) of a typical *h*-BN/*n*-MoS_2/p^+-MoS_2/*h*-BN all 2D heterostructure TFET. The heterostructure

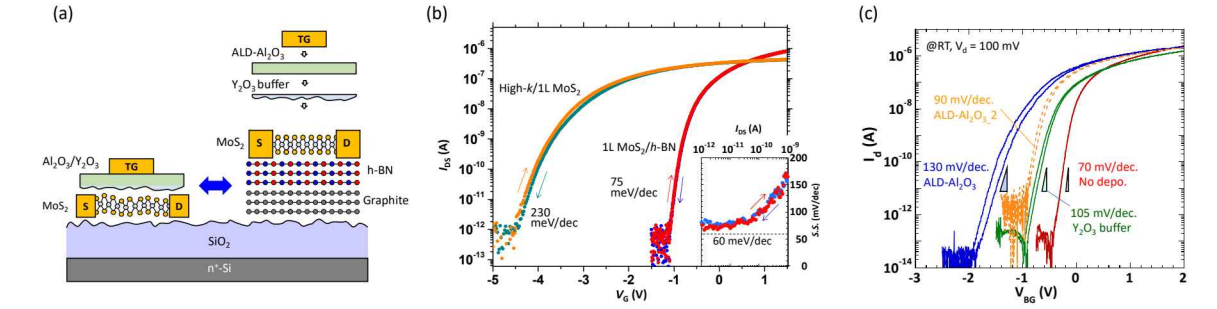

Fig. 1 a) Schematic illustration of two kinds of 1L-MoS_2 FET. One is FET with high-k top gate insulator, the other is heterostructure FET with h-BN and graphite. b) Transfer characteristics of two kinds of 1L-MoS_2 FET. The heterostructure MoS_2 FET shows better SS value. c) Transfer characteristics of 1L-MoS_2/h-BN FET before top-gate deposition (red), after Y_2O_3 buffer layer deposition (green), and after ALD-Al_2O_3 deposition (blue). Initially, back gate heterostructure 1L-MoS_2 FET was prepared and then top gate was deposited. The transfer characteristics were measured through the back gate. The back side MoS_2/h-BN interface was degraded by the top gate deposition, suggesting that top gate deposition may degrade

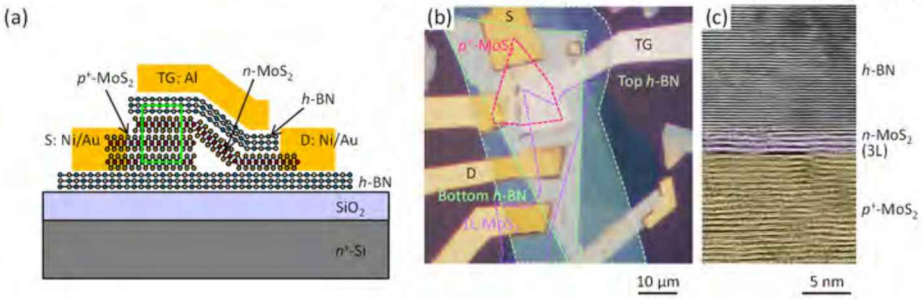

Fig. 2 a) Schematic illustration and b) optical micrograph of all 2D heterostructure TFET. c) Cross sectional TEM image of all 2D heterostructure at the solid rectangular in a). The number of MoS_2 layers is 3.

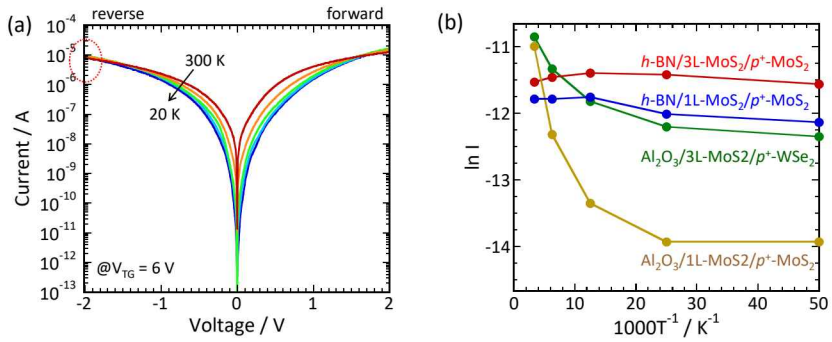

Fig. 3 a) Diode properties in the 3L-n-MoS_2/p^+-WSe_2 heterostructure at V_{TG} = 6 V and different temperatures (20, 40, 80, 160, and 300 K). b) Arrhenius plot of the current at the reverse bias of -2 V for different heterostructures.

device was prepared by pinpoint pickup and bubble free assembly technique.[4] The typical thickness for the top gate *h*-BN insulator and the p^+-MoS_2 source are ~15 nm and ~30 nm, respectively. The atomically sharp gate stack interfaces are clearly seen in the cross-sectional TEM image of Fig. 2c since all of the 2D materials are stable in air. As was expected, the diode properties of the all 2D heterostructure TFET with the 3L-*n*-MoS_2 channel in Fig. 3a shows the type III band alignment at V_{TG} = 6 V. The negative differential resistance (NDR) trend at the forward side is not visible. This could be explained by the suppression of the diffusion current due to the larger barrier between the conduction band minimum for p^+-MoS_2 and the valence band maximum for the *n*-MoS_2 channel because the E_G of bulk MoS_2 (~1.4 eV) is larger than the E_G of bulk WSe_2 (~1.2 eV). An Arrhenius plot of the current at the reverse bias of -2 V is compared with other heterostructures in Fig. 3b. It should be noted that all four heterostructure TFETs exhibit type III band alignment. For the *h*-BN top gate heterostructure devices with the 1L and 3L MoS_2 channels, temperature-independent behavior is evident over the entire temperature range, indicating that BTBT is dominant even at RT. This is quite promising for TFET operation with low SS values at RT. On the other hand, when Al_2O_3 was used as the top gate insulator, thermally activated behavior at high temperatures was clearly observed regardless of the source crystal. These comparisons indicate that the trap-related generation-recombination current [5] and/or the trap-assisted tunneling current under reverse bias are drastically suppressed by the successful integration of the electrically inert interface in the 2D heterostructure TFET.

Finally, the transfer characteristics of the 2D heterostructure TFETs at the reverse bias of -2 V at RT are shown in Fig. 4a. The estimated SS values are shown as a function of ID in Fig. 4b. For the 3L-*n*-MoS_2 channel, low *SS* value comparable with 60 $mVdec^{-1}$ of the Boltzmann limit was achieved at RT. Since the *SS* value for the 1L-*n*-MoS_2 channel was over 100 mV/dec, the smaller E_G of the 3L-*n*-MoS_2 channel was preferable. However, leakage current contributions should be considered carefully since artificially low SS values are often reported. We have confirmed that I_D overlaps with I_S for the 3L-*n*-MoS_2 channel because there is no gate leakage, which supports that the *SS* value is low comparable to 60 $mVdec^{-1}$ at RT.

4. Summary

The key finding regarding the quality of the heterointerface is that producing the defect-free clean heterointerface via integration of the *h*-BN top gate provides the BTBT dominant current even at RT. All 2D heterostructure TFETs produced by combining the type III *n*-MoS_2/p^+-MoS_2 heterostructure with the *h*-BN top gate insulator resulted in low SS values at RT.

References

[1] J. He, *et al.*, Adv. Electronic Mater. 2018, 4, 1800207.
[2] N. Fang, *et al.*, Adv. Func. Mater. 2019, 29, 1904465.
[3] A. M. Ionescu, H. Riel, Nature 2011, 479, 329-337.
[4] S. Toyoda, et *al.*, APEX 2019, 12, 055008.
[5] T. Gotow, *et al.*, J. Appl. Phys. 2019, 126, 214502.

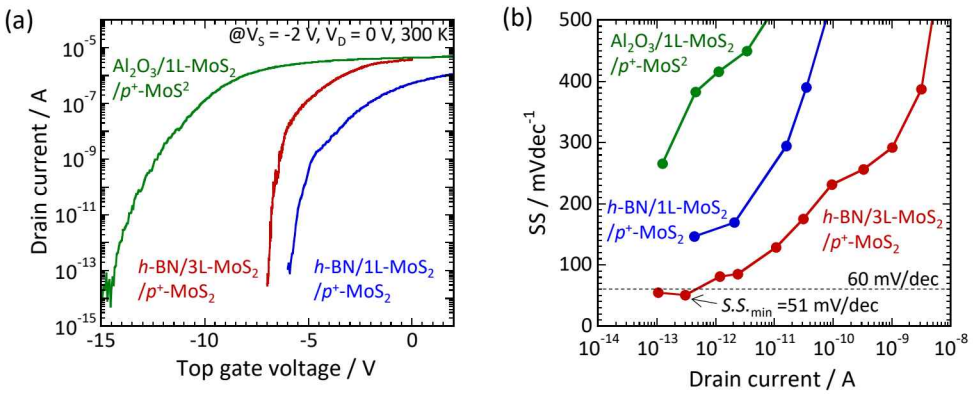

Fig. 4 a) Transfer characteristics for the three different heterostructure TFETs. b) SS as a function of I_D for the three different heterostructure TFETs.

Clean Energy Conversion Research Section

Hisayoshi Matsushima, Visiting Associate Professor
(Hokkaido University)

1. Introduction

Fusion reactor is one of the key technologies to achieve the zero-emission energy [1]. Hydrogen isotopes (hydrogen: H, deuterium: D, and tritium: T) are used as fuels in the reactor, but the present production process requires high energy consumption. For solving this problem, we have proposed the unique separation method, combined electrolysis and fuel cell (CEFC) [2]. Hydrogen and oxygen gases generated by water electrolysis are used for fuel cell as the power generation, while the hydrogen isotope separation is conducted. In fuel cell, the heavy isotopes are concentrated in the produced water, which can be returned to the electrolyte during the electrolysis [3].

The D separation by the aqueous solution and polymer electrolyte electrolysis has been reported [4]. It is suggested that the separation efficiency depends on the electrochemical kinetic factors, *ex.* hydrogen evolution reaction (HER). However, there are few papers about the fundamental study.

In molten salt, the HER occurs through the oxidation reactions of hydride ions (H^-) and deuteride ions (D^-), which is different from that in aqueous solution systems. That is, due to the difference in the HER mechanism, the high isotope separation can be expected. In addition, the electrochemical reaction rate can be increased due to the high temperature. The low overvoltage reduces the energy consumption of the separation system. Therefore, in the present project, a novel method using molten salt electrolysis is focused and the D separation is studied.

2. Electrochemical Measurement

In this study, experiments were conducted in the three electrodes system (Fig. 1). The chemicals were dried in vacuum environment at 723 K for 24 hours. They were mixed with the ratio of LiCl:KCl = 58.5:41.5 mol% and melted at 673 K. Three different electrode materials (Mo, Pt, Zn) were used for the working electrode, and a glassy carbon rod or an Al wire was used for the counter electrode. The reference electrode was an Al-Li alloy in an electrochemically formed (α + β) two-phase coexisting state. The potential was calibrated against the Li^+/Li electrode. The LiH and LiD were added to the molten salt at 1.0 mol% and 0.2-1.0 mol%, respectively.

Cyclic voltammograms (CV) with a several of potential scanning speeds was measured. Figure 2 shows the CV of the Mo electrode when LiD (0.4 mol%) was added in the LiCl-KCl molten salt. When the potential was scanned in the anodic direction, the

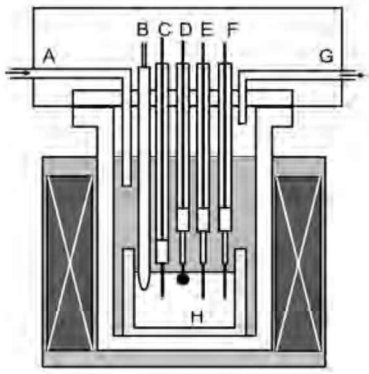

Fig. 1 Schematic illustration of experimental setup; (A) Ar gas inlet, (B) thermocouple, (C) counter electrode, (D) working electrode, (E) Al-Li wire reference electrode, (F) Al wire counter electrode, (G) gas outlet, (H) electrolyte.

oxidation peak associated with the deuterium evolution reaction (DER) was observed at 0.7-0.8 V *vs.* Li^+/Li. As the scanning speed was increased in the range of 0.2~5.0 V s^{-1}, the peak current increased and the peak shape was clearer. When the potential reached at 1.0 V, the scan direction was reversed to examine the reduction reaction. Interestingly unlike HER, the reduction current was hardly measured in DER. This may be explained by the low solubility of D_2 gas in the molten salt.

3. D Separation

The hydrogen gas during the potentiostatic electrolysis was discharged from the outlet with Ar

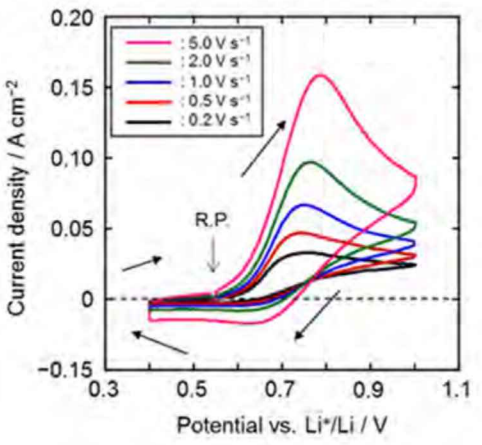

Fig. 2 Cyclic voltammograms of Mo electrode in LiCl-KCl-LiD (0.4 mol%) at various scanning rate.

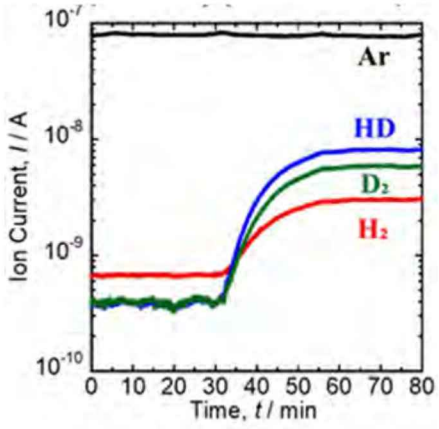

Fig. 3 QMS results of the hydrogen gas evolved from Mo electrode.

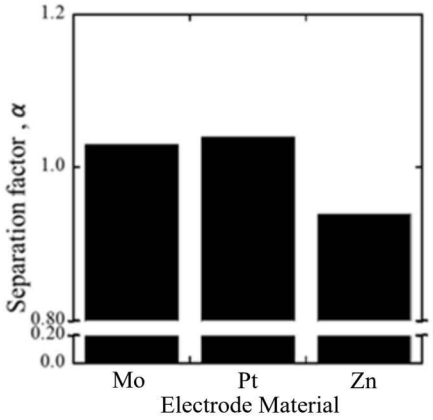

Fig. 4 Bar graph of separation factor at several electrode materials; Mo, Pt, and Zn.

carrier gas. It was introduced into a quadrupole mass spectrometer (QMS) for the gas analysis. Figure 3 shows the result of the QMS analysis, when the electrolysis was conducted at 0.7 V. The concentration of LiH and LiD was 1.0 mol%. The gas components were consisted of mass number $m = 2$ (H_2), $m = 3$ (HD), and $m = 4$ (D_2). Among the three gas mixtures, the ratio of HD gas was the largest, as seen in the water electrolysis in 10 at% D [4].

To quantitatively evaluate the separation, the separation factor, α, was defined in Eq. (1),

$$\alpha = \{[H]/[D]\}_g / \{[H]/[D]\}_m \quad (1)$$

where [L] is atomic concentration of the hydrogen isotopes (H and D), subscript of "g" is gas and "m" is molten salt. The atomic concentration in the hydrogen gas was calculated from the ion current of QMS by following equation,

$$[H]/[D]=[(i_{H2}\times 2+i_{HD}) /(i_{D2}\times 2+i_{HD})] \quad (2)$$

where i_x is the ion current of gas x.

The α value of the electrode materials are summarized in Fig. 4. For Mo and Pt electrodes, α was slightly larger than 1.0. This suggested that D was enriched in the electrolyte, as done by water electrolysis. On the other hand, for Zn electrode, the α value less than 1.0. That is, D was enriched in the generated hydrogen gas. This phenomenon was inverse against the well-known electrolysis process.

5. Summary

The hydrogen isotope separation by the molten salt electrolysis showed different behavior form the water electrolysis. This suggests that not only kinetic factors related to electrode reactions, but also the state of the dissolved gas differs among the isotopes. In the future, we will investigate the reduction reaction of the hydrogen isotopes on several electrode materials.

References

[1] E.S. Hanley, J.P. Deane, B.P.O. Gallachoir, *Renew. Sustain. Energy Rev.*, **82** (2018) 3027.
[2] R. Ogawa, R. Tanii, R. Dawson, H. Matsushima, M. Ueda, *Energy*, **149** (2018) 98.
[3] S. Shibuya, H. Matsushima, M. Ueda, *J. Electrochem. Soc.*, **163** (2016) F704.
[4] H. Matsushima, H. Sato, M. Ueda, H. Ito, *J. Electrochem. Soc.*, **166** (2019) F566.